geologica acta

Citation: Machek, M., Roxerová, Z., Kusbach, V., Kučeráková, M., Vratislav, S., 2025. Evolution of microstructure and texture in a small-scale high-temperature marble shear zone from the Ossa-Morena Zone (Iberian Variscan Belt). Geologica Acta, 23.24, 1-pgs. DOI: 10.1344/GeologicaActa2025.23.24

Online ISSN: 1696-5728

Evolution of microstructure and texture in a small-scale high-temperature marble shear zone from the Ossa-Morena Zone (Iberian Variscan Belt)

Matěj Machek[1] Zuzana Roxerová[1] Vladimír Kusbach[1] Monika Kučeráková[2] Stanislav Vratislav[2]

[1]Geophysical Institute v.v.i., Academy of Sciences of the Czech Republic
Boční II/1401, 141 31, Praha 4, Czech Republic. Machek E-mail: mates@ig.cas.cz

[2]Department of Solid State Engineering, Faculty of Nuclear Sciences and Physical Engineering, Czech Technical University in Prague
Břehová 7, 115 19 Prague, Czech Republic

ABSTRACT

This research investigates microstructures and crystallographic preferred orientation in a high-temperature Variscan small-scale shear zone within marbles from the south-western Ossa-Morena Zone (Iberian Variscan Belt). Quantitative microstructural analysis, and crystallographic preferred orientation data obtained via neutron diffraction and electron backscatter diffraction mapping allowed to infer the deformation mechanisms and active slip systems. The primary S2 foliation, formed during the Variscan D2 deformation phase, is characterized by high-temperature grain boundary migration recrystallization mechanism, coupled with intracrystalline slip on the c(0001)<-12-10> system. Ductile shear zone development, marked by a coarse-grained microstructure with pronounced shape preferred orientation parallel to the shear plane, involved both high-temperature grain boundary migration recrystallization and intracrystalline dislocation creep, accommodated by f{-1012} <10-11> and r{10-14} <-2021> slip systems. These results indicate a high-temperature extensional origin for the S2 foliation and the shear zone formation during the D2 deformation event of the Ossa-Morena Zone, linked to thermal effects from the Beja Igneous Complex plutonism and regional partial melting driven by asthenosphere upwelling (~353–335Ma).

KEYWORDS **Calcite microstructure. High-temperature shear zone. Crystallographic preferred orientation. Grain boundary migration recrystallization, deformation mechanism.**

INTRODUCTION

The reconstruction of a rock's deformation history and the tectonic evolution of geological units often relies on understanding the deformation mechanisms responsible for their structural characteristics. This requires detailed knowledge of how microstructure and texture develop during progressive deformation. Most deformation within the Earth lithosphere is concentrated in high strain ductile shear zones (*e.g.* Fossen and Cavalcante, 2017; Ramsay, 1980; Ramsay and Graham, 1970; Sibson, 1977). These shear zones provide critical insights into the tectonic reworking of the lithosphere (Fossen and Cavalcante, 2017). The rheological properties of rocks during shear zone evolution shape the resulting structural patterns (*e.g.* Carreras *et al.*, 2010; Fossen and Cavalcante, 2017; Ramsay, 1980). These structural patterns depend on the microstructural characteristics of the rock and on the pressure and temperature conditions of deformation, rate of displacement and the presence of fluid. Shear zones often

record progressive deformation under constant conditions (Means, 1995) that are optimal for analysing deformation mechanisms.

Carbonate rocks are widespread in diverse tectonic settings. As a result, the deformation behaviour of calcite, including its characteristic textures, microstructures, deformation mechanisms, and active slip systems, has been extensively investigated in experiments (*e.g.* Barnhoorn *et al.*, 2004; Barnhoorn *et al.*, 2005; De Bresser and Spiers, 1997; Marques *et al.*, 2015; Pieri *et al.*, 2001; Pieri *et al.*, 2001; Rutter *et al.*, 1994; Schmid *et al.*, 1987; Wenk, 2002) and in naturally deformed rocks across a broad range of temperature and strain conditions (*e.g.* Bestmann *et al.*, 2000; Bestmann *et al.*, 2006; Busch and van der Pluijm, 1995; de Bresser, 1989; Dietrich and Song, 1984; Erskine *et al.*, 1993; Kusbach *et al.*, 2019; Leiss and Molli, 2003; Oesterling *et al.*, 2007; van der Pluijm, 1991).

However, studies focusing on the microstructures and textures of naturally deformed marbles within high-temperature shear zones remain rare in the literature (Burlini *et al.*, 1998; de Bresser, 1989; Kurz *et al.*, 2000; Leiss and Molli, 2003; Schulmann *et al.*, 2023).

This study examines the evolution of microstructure and texture across a high-temperature shear zone in marble from the south-western Ossa-Morena Zone, a major Paleozoic tectonics unit of the Iberian Variscan belt. Through microstructural observations, quantitative microstructural analysis and crystallographic preferred orientation data obtained via neutron diffraction and electron backscatter diffraction mapping, we characterize the microstructural evolution, interpret the active deformation mechanisms and slip systems in the deformed marble, strain condition and discuss these findings regarding tectonic evolution.

GEOLOGICAL AND STRUCTURAL BACKGROUND

The investigated ductile Shear Zone (SZ) is located within the marbles of the Alvito-Viana do Alentejo region, which outcrops at the south-western Ossa-Morena Zone (OMZ) in the Iberian Variscan belt (Fig. 1). The OMZ represents a heterogeneous and complex tectonic unit that records successive tectonometamorphic events associated with the Cadomian and Variscan orogenic cycles (Quesada and Oliveira 2019; Rosas *et al.*, 2008). The Cambrian marbles of Viana do Alentejo (Moreira *et al.*, 2019) are part of the Cambrian-Ordovician siliciclastic and carbonate rift-related rock sequences (Chichorro *et al.*, 2008; Pereira *et al.*, 2007). These marbles have undergone at least three deformation phases and two thermal events during the Variscan orogen (Gomes, 2001; Pereira *et al.*, 2015; Pereira *et al.*, 2009; Rosas *et al.*, 2008).

The first Variscan deformation phase (D1) is attributed to a Late Devonian subduction-related high-pressure/medium-temperature event (1.0±0.1GPa and 470-510°C) (Akker *et al.*, 2020; Rosas *et al.*, 2008). In the Alvito-Viana do Alentejo region, evidence of D1 is rarely preserved in mafic rocks and is entirely overprinted by subsequent deformation in carbonates (Akker *et al.*, 2020; Rosas *et al.*, 2008). The second deformation phase (D2), during the Early Carboniferous, corresponds to low-pressure/higher-temperature conditions (0.6±0.2GPa and 550-800°C) and is associated with crustal extension and doming (Akker *et al.*, 2020; Gomes, 2001; Rosas *et al.*, 2008; Pereira *et al.*, 2009). D2 phase is followed by crustal thickening, which led to the folding of S2 foliation and the formation of S3 foliation. D3 is related to thrusting and strike-slip shear zones and is accompanied by retrogression at greenschist conditions (Dias da Silva *et al.*, 2018; Rosas *et al.*, 2008; Pereira *et al.*, 2009; Pereira *et al.*, 2022). Thermal events associated with plutonism occurred during the Variscan orogeny in the region: The emplacement of the Mississippian gabbro-diorite and granitic rocks Beja Igneous Complex (BIC) and the Beja-Acebuches amphibolites (Azor *et al.*, 2008: Akker *et al.*, 2020; Pin *et al.*, 2008; Rosas *et al.*, 2008; Pereira *et al.*, 2022) at the boundary between the OMZ and South Portuguese Zones. This magmatism is linked to D2 deformation and thermal metamorphism, accompanied by metasomatism of carbonate rocks in the Alvito-Viana do Alentejo region (Akker *et al.*, 2020; Gomes, 2001and Missisippian to Pennsylvanian Évora Massif gneiss dome (Akker *et al.*, 2020; Dias da Silva *et al.*, 2018; Pereira *et al.*, 2012). The Pennsylvanian intrusions either coincided or postdated the D3 compression-related low-temperature deformation (Dias da Silva *et al.*, 2018; Rosas *et al.*, 2008).

The Variscan structure in the immediate vicinity of the sampling site (Viana do Alentejo) is characterized by the superposition of two main foliations. Older foliation is coarse-grained, subhorizontal to gently dipping to the northeast and north characterized by coloured layering and symmetrical boudinage of more competent layers. This foliation is locally folded by open to tight folds and overprinted by medium angle to steep mylonitic foliation that dips toward the northeast. The structural superposition, characteristics, and orientation of the observed structures suggest their association with the D2 and D3 deformation events respectively.

The studied SZ (Fig. 2) sampled in an abandoned quarry south of the Viana do Alentejo (38.3237414N, 8.0122211W, SW Portugal, Fig. 1) exhibits normal sense of shear affecting the D2 foliation. The SZ is an isolated structure and no other similar structures are observed on the locality or in other quarries in the Viana do Alentejo region. The kinematics and characteristics of structural superposition suggests that the SZ developed in an extensional context

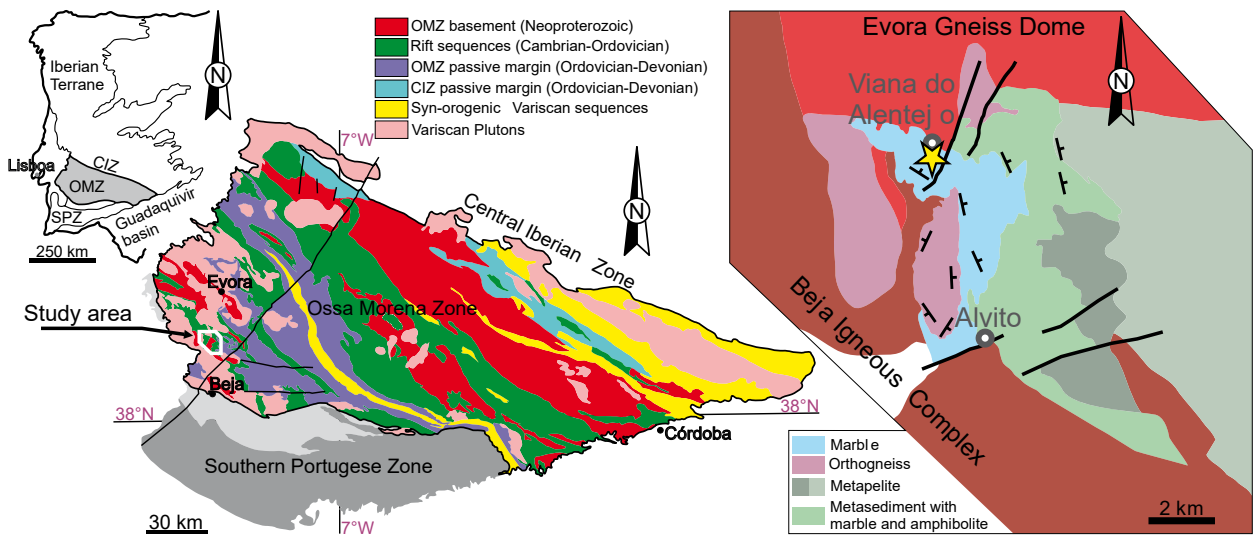

FIGURE 1. Geological overview map of the Ossa-Morena Zone and Viana do Alentejo region (simplified, modified from Akker *et al.*, 2020 who adapted it from Sánchez-García *et al.*, 2016 and Quesada, 2006) with Main terranes of southwestern Iberia modified after Akker *et al.*, 2020, Araújo *et al.* (2005), Ribeiro *et al.* (1990) and Quesada (1992). Central Iberian Zone (CIZ), Ossa-Morena Zone (OMZ), South Portuguese Zone (SPZ). The inset provides a geological map of the study area, indicating the precise locality of our research with a star symbol and orientation of foliation in the region after Akker *et al.* (2020).

and temporally coincided with the high-temperature D2 deformation associated with doming and plutonism. The orientation and HT character of the SZ suggests that the SZ predates the formation of the low-temperature, steep mylonitic foliation associated with the D3 deformation event. The main structural feature at the locality is a well-defined foliation, characterized by colour banding. From the boundary of the SZ, the main D2 foliation exhibits a progressive curvature towards the centre of the SZ, where most of the strain is localized (Fig. 2).

METHODS

This study examines the evolution of texture and microstructure within the marble SZ by integrating both quantitative and qualitative microstructural analyses, as well as Crystallographic Preferred Orientation (CPO) measurements by Electron Backscatter Diffraction (EBSD) and Neutron Diffraction (ND) methods and rock and mineral chemical analyses. An overview of the main samples and the methods applied to each subsample is provided in (Kusbach *et al.*, 2025a, b). The ND method was employed to obtain a representative CPO of calcite from the entire volume of the coarse-grained samples (cylindrical, approximately 2cm in length and diameter). The EBSD method, utilized in mapping mode, was applied to examine the grain structure and intracrystalline deformation features.

For purposes of this microstructural study the SZ was initially sampled across the strain gradient using a portable drilling machine. Oriented thin sections were cut perpendicular to the axes of the drilled cylinders for microstructural investigations. Qualitative description of the microstructure was examined using optical microscopy and photographed using Nikon Eclipse 80i optical microscope at the Institute of Geophysics, Academy of Sciences of the Czech Republic. For quantitative microstructural analysis, the thin sections were scanned employing polarizing foils to obtain high-resolution cross-polarized images. These images were manually digitized in the ESRI ArcMap environment to obtain a vector representation of the microstructure. Analysis of the resulting microstructural model was conducted using PolyLX, a python package for visualization and analysis of digitized 2D microstructures (Lexa *et al.*, 2024).

Whole rock chemical composition analyses were performed at Bureau Veritas Commodities Canada Ltd., Vancouver, using Inductively Coupled Plasma-Optical Emission Spectrometry (ICP-OES) and Inductively Coupled Plasma-Mass Spectrometry (ICP-MS).

Phase analyses by X-ray powder diffraction were performed with Empyrean PANalytical X-ray powder diffractometer using Cu radiation at the Institute of Physics of the Czech Academy of Science. Phase analysis of the powder sample was performed using the PANalytical High Score software package and PDF-5 structural database.

The phase chemical analyses and CPO maps were conducted using a Scanning Electron Microscope (SEM)

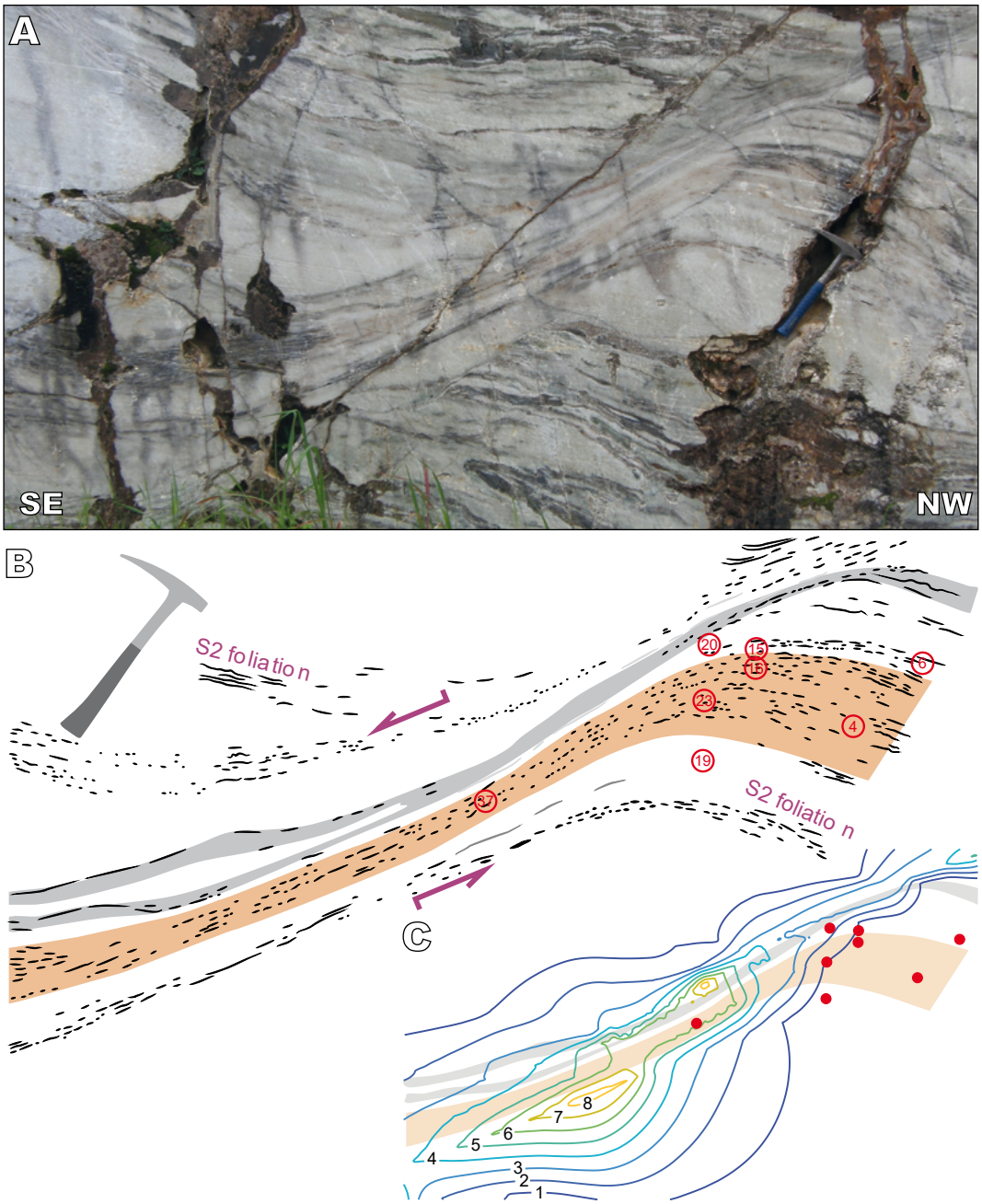

FIGURE 2. Detailed view of the studied SZ. A) Field photograph with a 33cm geological hammer for scale. B) Simplified structural sketch showing numbered drill core sample locations with marked S2 foliation and shear sense of the SZ. Black lines indicates the foliation traces and the grey and orange bands represent simplified colour structure of the section marking the shear zone. C) Strain analysis section of the SZ, with structural features and sample localities (red points) indicated.

coupled with an Energy Dispersive Spectroscopy (EDS) and Electron Backscatter Diffraction (EBSD) detectors. The instrument used is a Tescan Vega SEM equipped with EDS X-Max 50 and NordlysNano EBSD camera (Oxford Instruments) housed at the Laboratory of Scanning Electron Microscopy and Microanalysis, Institute of Petrology and Structural Geology, Faculty of Science, Charles University, Prague.

The neutron texture measurements were performed on the KSN-2 neutron diffractometer located at the horizontal channel of the LVR-15 research nuclear reactor at Institute of the Nuclear Research in Řež, Czech Republic. The used neutrons had wavelength $\lambda = 0.1362$nm, the ultimate resolution $\Delta d/d = 7 \times 10\text{-}3$ at the diffraction angle $2\theta = 19°$. To measure the calcite phase CPO, the samples were placed in a three-axis texture goniometer and the complete pole

figures for the planes (0006), (10-14), (11-20) and (11-23) of calcite were measured. All the obtained pole figures were used as input data to the MTEX MATLAB toolbox (Bachmann *et al.*, 2010). The estimation of the Orientation Distribution Function (ODF) in MTEX is based on a modified least squares estimator (Hielscher and Schaeben, 2008).

EBSD maps and ND data were processed using the MTEX 5.10.2 MATLAB toolbox (Bachmann *et al.*, 2010). The strength of CPO is characterized by texture index J and misorientation index M, which were calculated from the orientation distribution functions (Mainprice *et al.*, 2014; Skemer *et al.*, 2005). Based on the neutron diffraction data, the 3D plots of ODFs in Euler space and pole figures of main crystallographic directions and poles to planes were plotted. Additionally, grain structure was reconstructed from the EBSD data (misorientation angle ≥10°), and Misorientation Inverse Pole Figures (MIPFs) of subgrain-boundaries (<2°) were generated by plotting orientation of misorientation axes between neighbouring subgrains in the crystal coordinates system. This analysis is independent of the structure or strain orientation and directly characterizes the dislocations forming the dislocation walls that constitute the subgrain-boundaries.

RESULTS

The SZ is classified as a ductile shear zone by the absence of macroscopic fractures and exhibiting a continuous displacement gradient (Fig. 2A, B). No markers indicating deformation processes other than simple shear were observed, leading to the conclusion that simple shear deformation is the dominant deformation mechanism. The SZ can be followed on the quarry wall for approximately 3 meters, with both width and displacement varying along its trace. The maximum measured normal displacement (~100cm) along the SZ is approximately three times the maximal width (~35cm) of the SZ.

Strain analysis was performed under the assumption of simple shear as the exclusive deformation mechanism, utilizing the passive marker rotation method (Ramsay, 1983). First, eight traces of reoriented S2 foliation were produced on a grid with a 0.5cm interval from high-definition outcrop photography. Next, individual strain profiles for each foliation trace were generated, incorporating corrections for the mesoscopic waviness of the SZ. Outliers in each profile were identified, removed, and replaced with the average of neighbouring data points. The primary cause of outliers was the parallelism between the minor segments of the foliation traces and the main trace of the SZ. The rectified strain profiles were then interpolated using the natural neighbour method to create a continuous strain map (Fig. 2C) covering the region of interest. The maximum observed shear strain (γ) was 9.2.

For further analysis, the SZ area was divided into the three zones (Fig. I Appendix): Zone 0 - characterized by no visible deformation and only the primary S2 foliation with γ= ~0; Zone 1 - defined by the curved path of the primary S2 foliation with most samples γ in range between 0.2 and 2; Zone 2 - defined highly deformed fabric within SZ core parallel to the SZ orientation with majority of samples having γ> 3.

Petrography

The marble affected by the SZ is predominantly composed of calcite, which constitutes 67-98% of the rock. In addition to calcite, the rock contains significant amounts of wollastonite, quartz and diopside, with accessory amounts of datolite, scapolite and secondary hydroxyapophyllite as determined by SEM-EDS/microprobe analyses (Kusbach *et al.*, 2025a, b). The non-calcite mineral phases are primarily concentrated in thin, colored bands of fine-grained aggregates, which also include fine-grained calcite. These aggregates represent between 2% to 10% of rock volume, as determined through microstructural analysis. Diopside, quartz, and, in some cases, even wollastonite are also found at grain boundaries between large calcite grains or as inclusions within them. X-ray powder diffraction analysis revealed the presence of 0-13% of wollastonite, 1-18% quartz and 1-9% diopside in the studied marble (Kusbach *et al.*, 2025a,b). The whole-rock major-element composition is characterised by high amount of CaO (53.3-55.1wt%) and significant content of SiO_2 (1.29-8.92wt%), MgO (0.47-1.01wt%), MnO (0.11-0.19wt%) Fe_2O_3 (0.09-0.18wt%) and Al_2O_3 (0.08-0.14wt%).

Microstructure

The primary microstructure of the S2 foliation outside the SZ is characterized by the coarse-grained calcite, often exhibiting lobate irregular shapes (Figs. 3A, B; 4A, B) with highly lobate, interfingered and serrated grain boundaries (Fig. 3A, B). Small 'island' and 'left-over' grains, which are in optical continuity, are present within the calcite microstructure (Fig. 3E). Calcite grains of all sizes display I and II type twinning (Burkhard, 1993). In some cases, the grain boundaries of calcite are pinned by small grains of diopside or quartz (Fig. 3C, D). The fine-grained aggregates also appear to pin the calcite grain size along the aggregate bands. These fine-grained aggregates consist of wollastonite, larger grains of diopside and quartz (Fig. 3M, N). The wollastonite within the aggregates predominantly exhibits a granoblastic polygonal microstructure.

The calcite microstructure in the SZ (Fig. 4D-G) is characterized by a reduced presence of large and highly

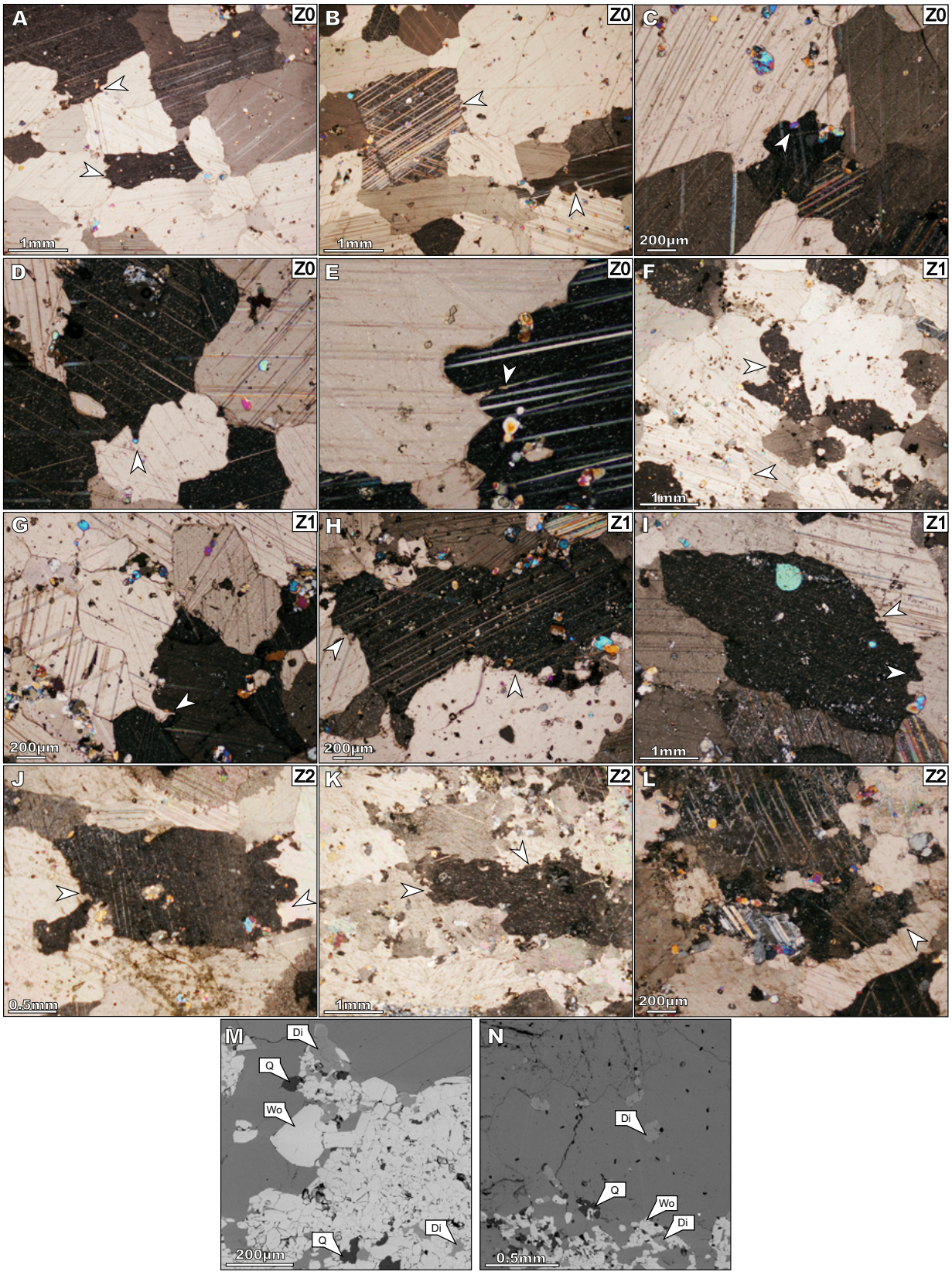

FIGURE 3. Photomicrographs and BSE images illustrating the microstructural features and their relationships in individual strain intensity zones. A-E) Zones 0-2, F-I) Zone 1, J-L) Zone 2. A, B, F-J) Lobate, interfingered and serrated grain boundaries. C-D) Grain boundaries pinned by small diopside grains. E) 'Left-over' calcite grain. M-N) BSE images of fine-grained aggregates microstructure.

lobate grains. Lobate, interfingered and serrated grain boundaries, grain boundaries locally pinned by small grains of diopside or quartz, and 'island' grains are prevalent throughout the microstructure, even in the parts of the highest documented strain within the centre of the SZ (Figs. 3F-L, III Appendix). With increasing shear strain, more grains with straight grain boundaries and 120° triple points are observed, with some grains exhibiting significant elongation (Fig. 4D-G). Additionally, calcite grains within the SZ contain optically distinguishable subgrains. The microstructure of the fine-grained aggregates observed under an optical microscope appears consistent with that observed outside the SZ, characterized predominantly by a granoblastic polygonal microstructure of wollastonite (Fig. 3M).

Quantitative microstrustructural analysis

Three quantitative parameters were used to analyze the grain-size and shape evolution of the microstructure across the strain gradient in the SZ describe the evolution of microstructure within the SZ (Fig. 5). The grain size is represented by the Equal Area Diameter (EAD), while the shape of the grains is described using the Aspect Ratio (AR) and PARIS factor. The EAD is defined as the diameter of a circle that has the same area as the grain. The AR is the ratio of the long axis to the short axis of an ellipse fitted to the grain`s outline. The PARIS factor quantifies the lobateness (convexity or concavity) of grain boundaries, expressed as a percentage of the average relative indented surface fraction, as outlined by (Panozzo, 1983). The PARIS factor of 0% corresponds to a strictly convex shape, with increasing values indicating increasing lobateness, having no upper limit.

The grain size outside the SZ (Zone 0) displays a broad, right-skewed distribution, characterized by mean value 0.96mm, a mode of 0.47mm, and a maximum grain size of 5mm (Fig. 5A). The grain size distribution indicates a significant population of grains larger than 1mm. The distribution of axial ratio values outside the SZ has a mean of 1.78 and a mode of 1.45, with most values falling below 4, except one outlier grain (Fig. 5G). The PARIS factor of grain boundaries shows a mean value at 15.46% and a mode at 5.77%, with a significant proportion of grains exhibiting the PARIS greater than 25% (Fig. 5A, G). Additionally, the lobateness of calcite grains outside the SZ demonstrates clear positive correlation with grain size. Furthermore, large grains with EAD exceeding 1 mm tend to exhibit statistically lower AR.

With increasing shear strain towards the centre of the SZ (Zone 1), the grain size distribution becomes tighter, exhibiting a smaller proportion of coarse grains and decreasing mean, median and mode values (Fig. 5B, C, D, G). The gradual change in grain size distribution towards the SZ core (Zone 2) is further evidenced by a decreasing difference between mean and mode values (Fig. 5E, F, G). In the SZ (Zone 2), the grain size distribution also reveals a secondary peak, indicating a significant population of grains with equivalent EAD between 0.7 and 0.8mm. With increasing strain, grain lobateness, as quantified by

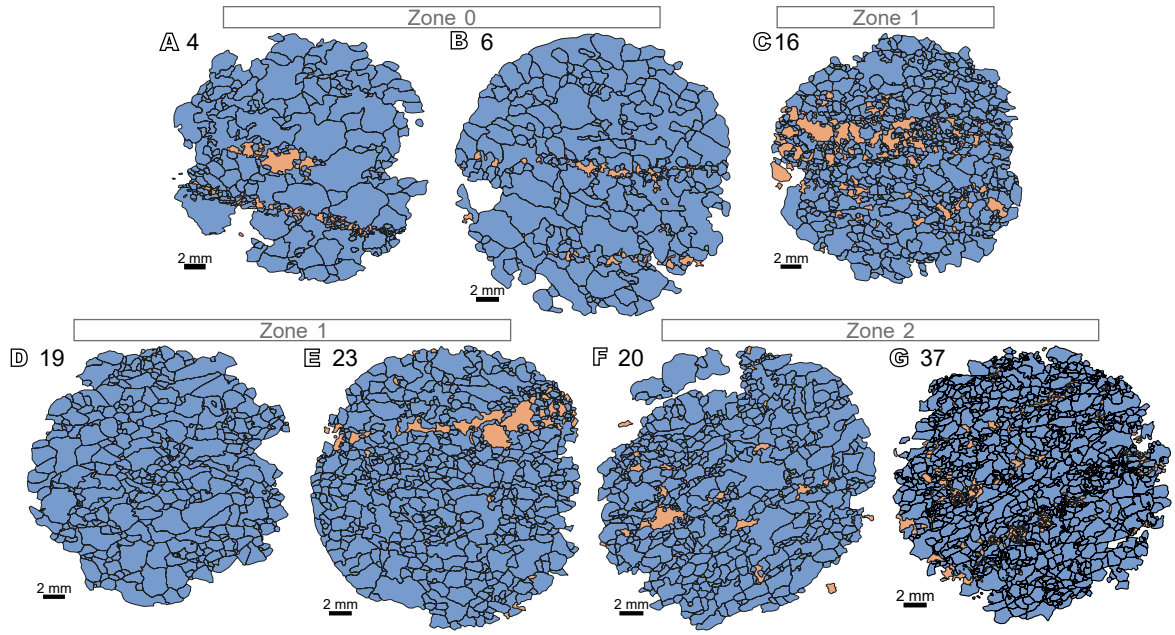

FIGURE 4. Traced microstructural and textural images of individual samples, arranged in strain intensity zones. The main rock (blue) is calcite, with variably distributed coloured bands of fine-grained aggregates (orange).

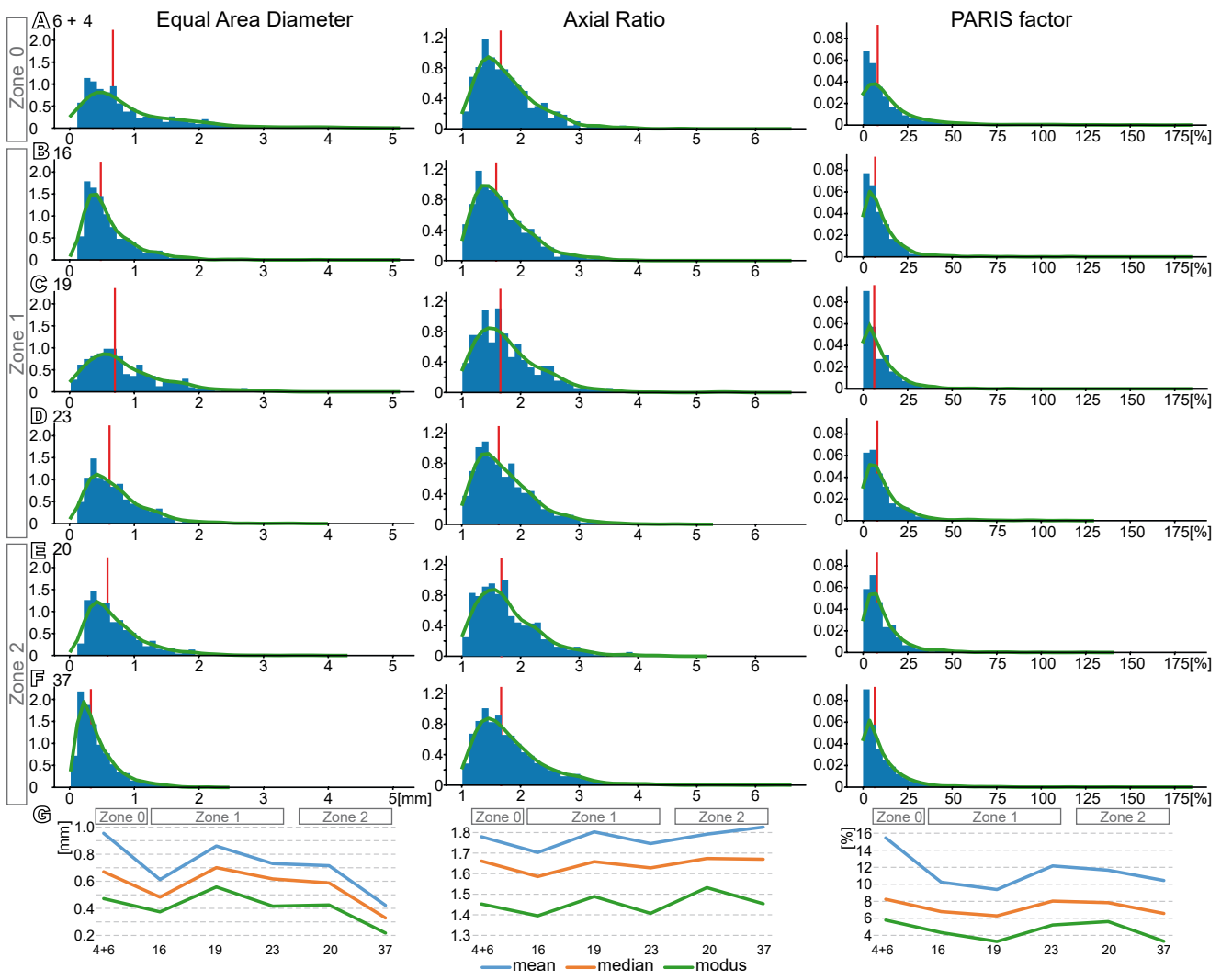

FIGURE 5. Quantitative microstructural analysis (grain size and shape) using Equivalent Area Diameter (EAD), axial ratio and PARIS factor. Red lines indicate mean values. Data are arranged by strain intensity zones (Zones 0-2). The lower panel displays the mean, median, and mode for each parameter across the strain zones.

the PARIS factor, shows a decreasing trend in both mean and mode values. Initially, this trend is accompanied by a decrease in the difference between these values; however, within the SZ core (Zone 2), this difference increases due to a disproportionate decrease in the mode value. Although the PARIS factor maintains a positive correlation with grain size with increasing strain, this correlation weakens approaching the SZ core (sample 20, Zone 2, Fig. 5E) and becomes questionable within the SZ core (sample 37, Zone 2, Fig. 5F). The axial ratio of calcite grains remains relatively constant, with only a slight increase in the SZ core.

A deviation from the described trend is observed in sample C1-16 (Zone 1), which exhibited the largest proportion (10%, as traced from the thin section) of fine-grained aggregate within its microstructure. This sample shows lower values for all three selected quantitative parameters, as well as smaller differences between the mean and mode value of the parameter distribution.

The Shape and Grain Boundary Preferred Orientations (SPO and GBPO) of calcite grains and fine-grained aggregates were analysed using fitting of ellipse to the grains and aggregates outlines and using PAROR and SURFOR methods (Panozzo, 1983, 1984).

Outside the SZ (Zone 0), the SPO and GBPO of calcite (Fig. 6A, B), as well as fine-grained aggregates exhibit angular deviation of up to 20° from the observed macroscopic fabric. Moreover, the preferred orientation of fine-grained aggregates does not coincide with that of

the calcite. Within Zone 1 (Fig. 6C), defined by the curved path of the primary foliation, the angular deviation between the macroscopic fabric and SPO and GBPO of calcite decreases, although the distinct aggregate orientation persists. At the core of the SZ (Zone 2, Fig. 6G) the SPO and GBPO of both calcite and aggregates become parallel to the macroscopic S2 foliation. The intensity of SPO and GBPO, as expressed by the minimum values of PAROR and SURFOR functions, remain constant irrespective of the documented strain value. A weak correlation between SPO and other quantitative parameters is observed only for the axial ratio of calcite grains. Grains exhibiting the highest AR are tending to be oriented subparallel to the average orientation of all calcite grains.

Crystallographic preferred orientation

Calcite

Calcite CPO determined by neutron diffraction is presented as ODFs in Euler angle space (Fig. II Appendix) and as pole figures for main crystallographic directions (Fig. 7).

The CPO of S2 foliation samples (Zone 0) is characterized by multiple ODF fibre components (Fig. II Appendix). These components are defined by submaxima of c-axes, which form a girdle perpendicular to the macroscopic foliation (Fig. 7A). This relatively strong c-axes preferred orientation is accompanied by weak preferred orientations of other main crystallographic directions (Fig. 7A).

Into the zone 1, a new ODF component that gradually modifies the calcite texture, developing single ODF component (Fig. II Appendix). The new texture is characterized by an elongated single maximum of c-axes, rotated approximately 30° counter clockwise from the pole to the SZ plane, consistent with the SZ kinematic. The CPO also exhibits a girdle of r-axes submaxima immediately surrounding the strong c-axes maximum and a girdle of a-axes parallel to the SZ plane (Fig. 7). The texture strength is relatively low and remains constant across the strain gradient, indicated by low J and M index values. Only at the SZ core, the M index slightly increases (Table I Appendix).

Detailed analysis of EBSD maps revealed an increase in the intensity of calcite intracrystalline deformation with intensifying shear strain, manifested by a rising number of low-angle (1°) subgrains, primarily formed around grain edges (Fig. III Appendix). Despite this, higher-angle subgrains (2° and 5°) remain rare, even in samples from the SZ core, which records the highest strain. The development of low-angle subgrains does not lead to the formation of new recrystallized grains or a core-and-mantle microstructure. The nature of the intracrystalline deformation is further documented by analysis of the subgrain-boundary

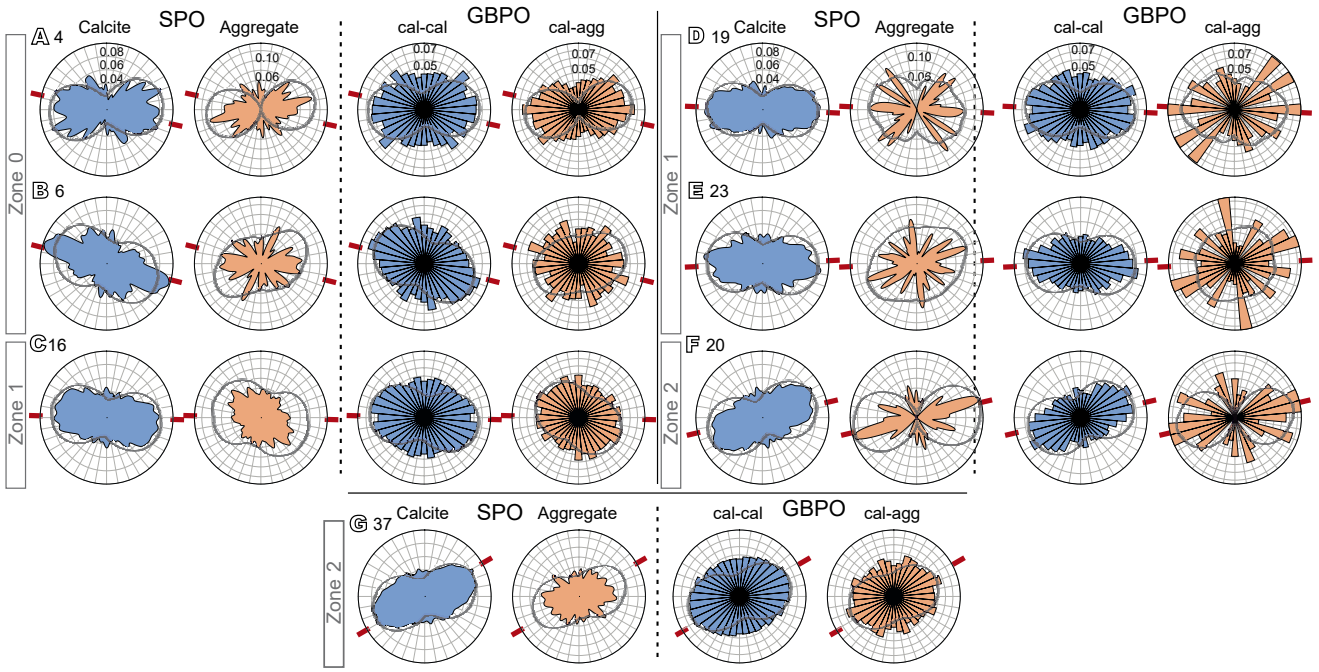

FIGURE 6. SPO and GBPO of calcite grains and fine-grained aggregates. The data are displayed in rose plots (probability density) weighted by individual long grain axes and arranged by strain intensity zones. Red lines at the diagram edges indicate the macroscopic fabric orientation. Data were analysed using fitting of ellipse to the grains and aggregates outlines, and PAROR and SURFOR methods (Panozzo, 1983; Panozzo, 1984). PAROR function: middle value 0.7, marginal value 1. SURFOR function: middle value 0.65, marginal value 0.95. The scale is marked only on the first row. The plots span from 0 to 360°.

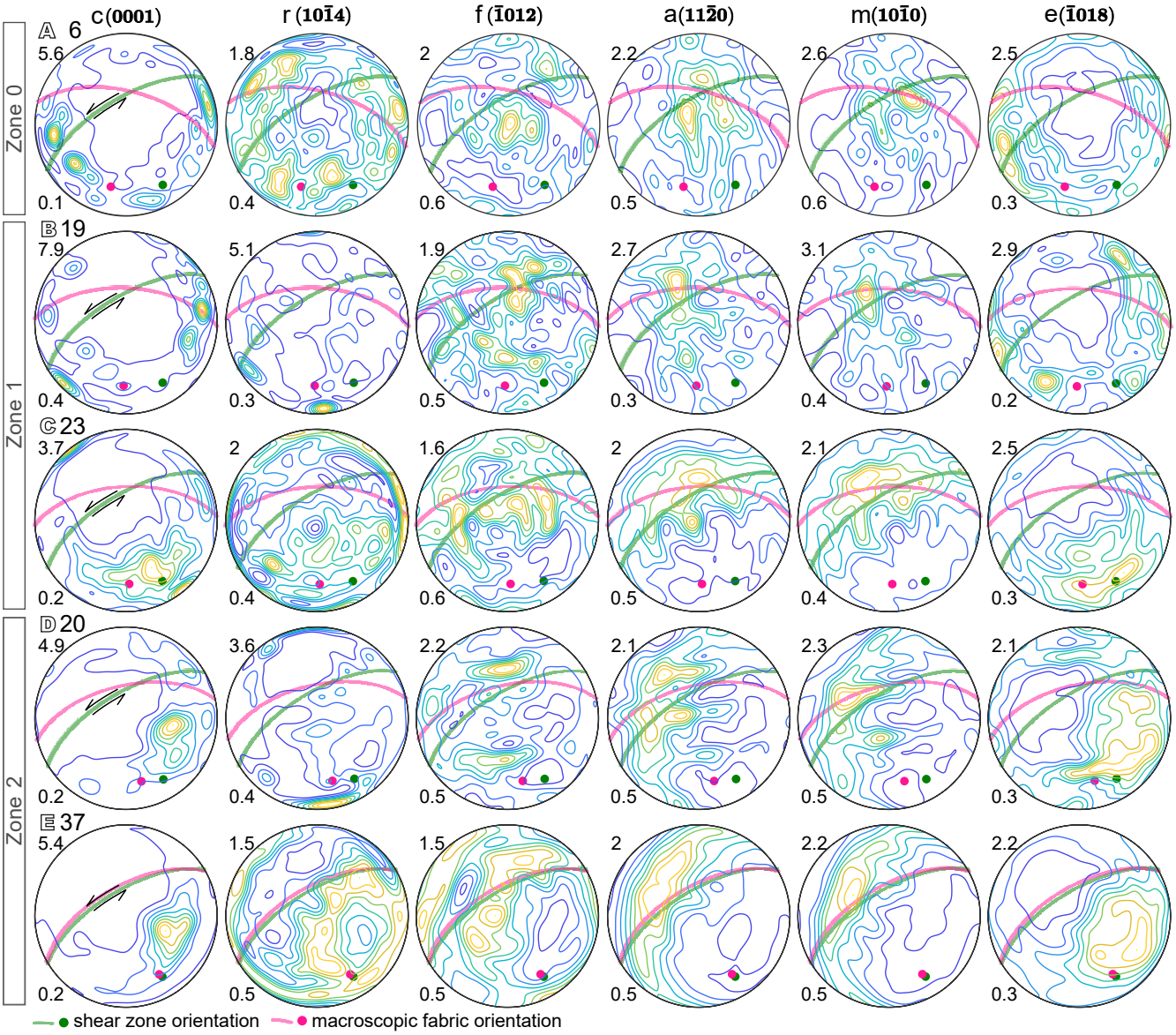

FIGURE 7. CPO pole figures for main crystallographic directions, arranged by strain intensity zones (0-2). Green lines and points indicate SZ orientation and poles; red lines and points indicate macroscopic fabric orientation and poles. Maximum and minimum multiples of random distribution (m.r.d.) are noted for each pole figure. In all pole figures the CPO is illustrated by 8 contours evenly distributed between minimum and maximum.

misorientation axis distribution in MIPFs (Fig. 8). In the undeformed sample (Zone 0), misorientation axes exhibit a pronounced maximum aligned with the <c> axis direction (Fig. 8A). With increasing strain (Zone 1), misorientation axes centred along the <a> and <m> directions appear (Fig. 8B, C). In the sample 37 from the SZ center (Zone 2, Fig. 8D, E), misorientation axes centred along the <a> direction clearly dominate (Fig. 8E).

Secondary phases

The low modal abundance of secondary phases (wollastonite, diopside and quartz) in the studied rock prevented the determination of their CPO using the ND method. Statistically robust texture analysis via EBSD requires a sufficient number of individual grain measurements for each mineral phase. Consequently, clearly interpretable quartz CPO, characterized by a c-axis girdle aligned with the macroscopic fabric, was only observed in sample 23 (n≈ 400) from the EBSD dataset (Fig. IV Appendix). Quartz CPO data from remaining samples were considered statistically insufficient for reliable interpretation.

The CPO of wollastonite and diopside is in all analysed samples weak to nearly random (Fig. IV Appendix). Despite the weak diopside CPO, EBSD maps of larger diopside

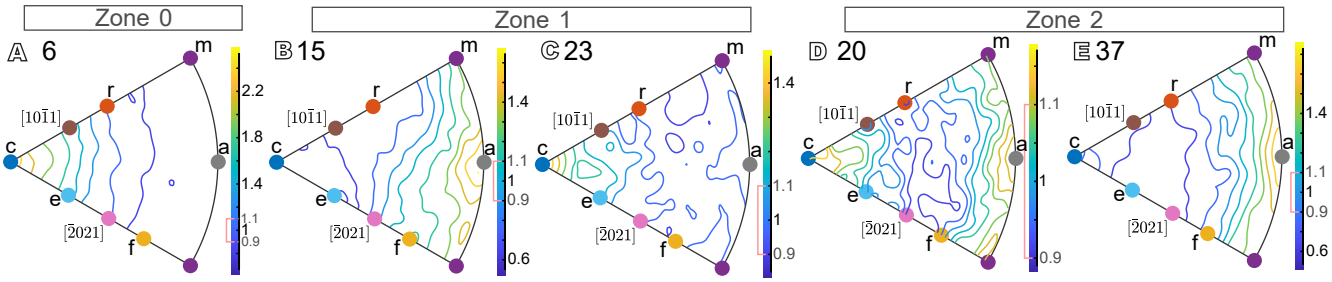

FIGURE 8. Subgrain-boundary misorientation axis analysis of calcite intracrystalline deformation, categorized by strain intensity zones (Zones 0-2) in Misorientation Inverse Pole Figures (MIPFs). Labels in MIPFs indicate crystal directions or plane normals. In all MIPFs the misorientation is illustrated by 8 contours evenly distributed between minimum and maximum. Contours are colored based on scale bars placed next to the MIPFs. Refer to the text for further discussion.

grains reveal evidence of intracrystalline deformation in the form of numerous subgrains. Moreover, an indirect record of diopside CPO development during the SZ formation is observed in the anisotropy of magnetic susceptibility. The A nisotropy of magnetic susceptibility (AMS), primarily carried by diopside in the studied marbles, follows the macroscopic fabric reorientation and is more pronounced in the samples with fewer fine-grained aggregates (Roxerová, 2025). Grain reconstruction based on EBSD mapping shows no SPO of the secondary phases (Fig. IV Appendix).

DISSCUSSION

To interpret the acting deformation mechanisms and conditions recorded in the S2 foliation and the SZ structural and microstructural observations quantitative microstructural analysis, and CPO measurements are integrated. Finally, the regional geological significance of these findings is discussed.

Conditions of deformation

The regional foliation and shear zone development, evidenced by structural and microstructural analyses, occurred during the Early Carboniferous D2 deformation event. This deformation event, associated with crustal extension and doming, is constrained to medium-pressure/higher-temperature (0.6-0.2GPa and 550-800°C; Akker 2020; Gomes 2001; Rosas 2008). A prolonged high-temperature event, concurrent with the D2 deformation, is attributed to the Mississippian High Temperature-Low Pressure (HT-LP) metamorphism (550-600°C; Akker *et al.*, 2020), linked to asthenosphere upwelling that caused continental crustal heating and partial melting. This regional scale event was locally influenced by thermal contact metamorphism from the BIC (~353-345Ma; Akker *et al.*, 2020; Pin *et al.*, 2008; Rosas *et al.*, 2008). This thermal metamorphism also resulted in metasomatism of carbonate rocks in the Alvito-Viana do Alentejo region, leading to the formation of wollastonite-rich aggregates (Akker, 2020; Gomes, 2001). Given that wollastonite formation in siliceous limestones from calcite and quartz occurs between 400-650°C (Ganino *et al.*, 2014), the temperature responsible for the studied SZ is estimated to be approximately 600°C.

Deformation mechanisms and crystal plasticity

To interpret the calcite deformation mechanisms operating during the SZ development, we integrate microstructural observations and quantitative microstructural analysis with the analysis of CPO obtained both from large samples using ND and conventional thin section EBSD maps.

The primary S2 foliation composed of predominantly lobate calcite grains of large grain size with serrated grain boundaries, a texture defined by several submaxima of c-axes forming girdle perpendicular to the macroscopic foliation in combination with a maximum of subgrain misorientation of the axes centred in the direction of the <c> axis, suggests its formation at high-temperature under prevailing pure shear deformation (Leiss *et al.*, 2003; Wenk *et al.*, 1987). The preservation of complex grain shape and grain boundaries suggests a limited influence of post deformation annealing at high-temperature (Barnhoorn *et al.*, 2005; Piazolo *et al.*, 2007).

The formation of lobate irregular grain shapes, serrated grain boundaries and small "island" or "left-over" grains in both primary S2 foliation, as well as in the core of the SZ. Calcite grains exhibit relatively constant and high aspect ratios and only limited grain size reduction with increasing shear strain and tight grain size distribution. The degree of SPO and GBPO of calcite grains remains relatively constant across the strain gradient, although the preferred orientation of grain shapes and grain boundaries aligns parallel to the macroscopic foliation within the SZ. The occurrence of these features indicates high mobility of grain boundaries

during deformation and stabilization of grain size towards equilibria. A well-defined CPO with constant and rather weak strength across the strain gradient is accompanied by intracrystalline deformation as evidenced by subgrain formation. This indicates the activity of dislocation creep within the grains. The observed microstructure across the SZ pointing to the high grain boundary mobility together with development of well-defined but weak CPO is a typical result of high-temperature Grain Boundary Migration (GBM) recrystallization (Guillope, 1979; Leiss, 2003; Molli, 2000; Pieri, 2001; Stipp, 2002; Urai, 1986) assisted by intracrystalline dislocation creep. High-temperature GBM recrystallization typically does not create a new grain size fraction of grains, because is driven by relative difference in dislocation densities between neighbouring grains, generating a driving force to reduce the overall strain energy (*e.g.* Poirier, 1985; Stipp *et al.*, 2002; Urai *et al.*, 1986). Consequently, grains with lower dislocation densities migrate into the grain with a higher dislocation density. In contrast, low-temperate GBM (Bulging recrystallization) produces very fine recrystallized grains along grain boundaries, cleavage planes and twin boundaries (*e.g.* Bestmann & Prior, 2003; Stipp *et al.*, 2002). The commonly observed mechanism of subgrain rotation recrystallization (SGR) in deformed calcite rocks (*e.g.* Barnhoorn *et al.*, 2004; Bestmann *et al.*, 2003; De Bresser *et al.*, 1997; Marques *et al.*, 2015; Oesterling *et al.*, 2007; Pieri *et al.*, 2001; Schmid *et al.*, 1980) is unlikely to operate during the SZ evolution due to only limited grain size reduction, significantly smaller subgrains sizes than the size of newly formed calcite grains, and the absence of core and mantle microstructure typical for the SGR recrystallization mechanism.

The subgrain boundary misorientation axes parallel to the pole of c plane in the primary microstructure outside the SZ (Zone 0, Fig. 8) indicate twist boundaries parallel to the (0001) plane formed by <-12-10> screw dislocations, which are likely generated by the activity of the c(0001)<-12-10> slip system (Ohl *et al.*, 2021) operating in experiments performed at temperature between 600-800°C (De Bresser *et al.*, 1997).

The occurrence and progressive predominance of misorientation axes in the <a> direction with increasing strain suggests subgrain boundaries formed by edge dislocations that arise due to activity of slip systems f{-1012}<10-11> or r{10-14}<-2021> (Ohl *et al.*, 2021). In experiments, the f<10-11> slip system activates between 600-800°C and r<-2021> slip system between temperatures ranging from 300°C to 800°C. The additional concentration of misorientation axes along <m> indicates the activation of more than one slip system during the GBM recrystallization and SZ formation. At high-temperature, the r<-2021> slip system exhibits lower critical resolved shear stress than the f<10-11> slip system (De Bresser *et al.*, 1997) suggesting a more likely dominant activity of the former. However, the observed synthetic rotation of the poles to c(0001) planes with the shear sense in pole figures has been in viscoplastic self-consistent models attributed to the significant activity of the f<10-11> slip system along with activity of the r<-2021> slip, without c<-12-10> slip being active (Barber *et al.*, 2006).

The observed synthetic rotation of poles to c planes with respect to shear sense is only rarely reported in both natural and experimentally deformed calcite aggregates (Fernández *et al.*, 2016). Commonly, the poles to the c planes exhibit antithetic rotation at low-temperature (Leiss 2003; Wenk, 1987) or align perpendicular to the shear plane at high-temperature (Pieri *et al.*, 2001). As demonstrated by the modelling of Barber *et al.* (2006), this observed texture pattern may indicate significant activity of the f<10-11> slip system. Furthermore, the microstructural evolution of deformed calcite aggregates can be influenced by the presence of secondary phases (Austin *et al.*, 2014; Ebert *et al.*, 2008; Rybacki *et al.*, 2014) and the activity of water or CO_2 during deformation (De Bresser *et al.*, 2005; Schenk *et al.*, 2005).

The atypical calcite CPO pattern observed within the SZ is attributed to a combination of: i) the high-temperature GBM, resulting in a coarse-grained microstructure with a strong SPO parallel to the shear plane; ii) intracrystalline dislocation creep accommodated by the activity of the f{-1012}<10-11> and r{10-14}<-2021> slip systems and iii) the presence of weak aggregates of secondary phases, dominated by fine-grained wollastonite.

Secondary phases

The fine-grained wollastonite, both outside and within the SZ, exhibits granoblastic polygonal microstructure and lacks CPO as well as SPO. This observation contrasts with previous studies indicating that wollastonite deformation typically generates strong CPO through a combination of dislocation creep and oriented growth (Elyaszadeh *et al.*, 2017). In the SZ, the SPO of whole secondary phase aggregates corresponds to that of calcite, being parallel to the shear plane. This suggests that these aggregates underwent the same type and intensity of deformation. However, the intracrystaline deformation is observed solely in diopside grains, representing the hard phase, which develops a weak CPO, as evidenced by the evolution of AMS (Roxerová *et al.*, 2025). While these results are not entirely conclusive, we propose that the microstructure characteristics of the secondary phase aggregates suggest that deformation was primarily accommodated by grain size sensitive diffusion-controlled creep of wollastonite (Bestmann *et al.*, 2003; Boullier *et al.*, 1975; Stünitz *et al.*, 1993). The fine-grained

aggregate of granoblastic polygonal wollastonite formed within the S2 foliation and was rotated into the SZ to align parallel to the shear plane.

Regional implications

The evolution of calcite microstructure and texture in the studied high-temperature SZ is characterized by a gradual fabric transformation. This fabric transformation is manifested by a progressive but limited reduction in grain size, narrowing of the grain size distribution, replacement of the primary ODF components with a single deformation-related component, and a loss of subgrains with misorientation axes centered in the <c> direction. While the microstructure analysis alone cannot definitively distinguish between primary and newly formed recrystallized grains, the combined textural and microstructural characteristics suggest that the fabric transformation from pure shear - dominated S2 foliation to the simple shear - dominated in the SZ was completed as deformation progressed towards core of the SZ. Therefore, we interpret the microstructure of the SZ determined by the combination of high-temperature GBM recrystallization mechanism accommodated by activity of intracrystalline dislocation creep at f{-1012} <10-11> and r{10-14}<-2021> slip systems in equilibrium with the temperature and deformation condition.

The results of the microstructural study of the marbles from Viana do Alentejo confirm the high-temperature extensional origin of the D2 foliation and the formation of the SZ is linked to the thermal event associated with high-temperature event, concurrent with the D2 deformation associated with the asthenosphere upwelling and (thermal) contact metamorphism with plutonic rocks of the BIC and the Beja-Acebuches amphibolites (~353-345 Ma; Azor *et al.*, 2008; Akker *et al.* 2020; Pin *et al.* 2008; Rosas *et al.* 2008). The high-temperature event likely had a relatively short duration in the studied area, as neither primary nor SZ microstructures exhibits evidence of post-deformation high-temperature annealing. Moreover, it is likely that the later thermal event related to granodiorite intrusions in the Évora Massif gneiss dome (320-313Ma; Akker, 2020; Dias da Silva, 2018; Pereira, 2012) did not significantly affect the studied region.

CONCLUSIONS

In order to reconstruct part of the deformation history of the marbles from the southwestern Ossa-Morena Zone in Portugal, we analyzed the evolution of microstructure and texture in small-scale Variscan high-temperature shear zone. By integrating diverse microstructural and textural analysis, we determined the dominant deformation mechanisms responsible for the structural record and correlated them with the tectonic evolution.

The primary fabric shows evidence of high-temperature GBM deformation accommodated by intracrystalline activity of the c(0001) <-12-10> slip system, as indicated by subgrain boundary misorientation axes preferred orientation. This, coupled with the microstructural characteristics, suggests that the primary microstructure formed at temperatures between 600-800°C.

The synthetic rotation of the poles to c planes with the shear sense, observed in the SZ's microstructure and texture, are explained by a combination of the high-temperature GBM recrystallization, which resulted in coarse-grained microstructure with strong SPO parallel to the shear plane, intracrystalline dislocation creep accommodated by activity of f{-1012} <10-11> and r{10-14} <-2021> slip systems, and the presence of weak aggregates of fine-grained wollastonite.

The results support the interpretation that the S2 foliation formed under high-temperature extensional conditions, and that the associated SZ developed during the D2 deformation event, driven by the thermal event related with lithosphere thinning, asthenosphere upwelling and plutonism, that occurred in this region of the Variscan orogen during the Mississippian.

DATA AVAILABILITYS

All data including Neutron diffraction measurement, EBSD maps, traced microstructure, and whole rock chemical composition generated and analysed during the presented study are available in the World Data Centre PANGAEA repository (Felden, 2023; Kusbach, 2025a).

ACKNOWLEDGMENTS

Martin Racek is acknowledged for assistance with SEM/EBSD measurements. Thanks to Fernando G. Marques for introducing the authors to the field of the Viana do Alentejo region. M.F. Pereira and F.J. Fernández are thanked for their useful comments and GeA editor A. Azor for editorial handling. The work of all authors was funded by the Czech Science Foundation Grant 22-12828S. Z.R., V.K.K. and M.M., were also supported by the Czech Academy of Sciences institutional support to the Institute of Geophysics of the Czech Academy of Sciences (RVO 67985530).

REFERENCES

Akker, I.V., Tajčmanová, L., Marques, F.O., Burg, J.P., 2020. U-Pb zircon geochronology and phase equilibria modelling of HPLT rocks in the Ossa Morena Zone, Portugal. International

Journal of Earth Sciences, 109, 2719-2738. DOI: https://doi.org/10.1007/s00531-020-01921-w

Araújo, A., Fonseca, P., Munhá, J., Moita, P., Pedro, J., Ribeiro, A., 2005. The Moura Phyllonitic Complex: an accretionary complex related with obduction in the Southern Iberia Variscan Suture. Geodinamica Acta, 18, 375-388.

Austin, N., Evans, B., Rybacki, E., Dresen, G., 2014. Strength evolution and the development of crystallographic preferred orientation during deformation of two-phase marbles. Tectonophysics, 631, 14-28. DOI: http://dx.doi.org/10.1016/j.tecto.2014.04.018

Azor, A., Rubatto, D., Simancas, J.F., González Lodeiro, F., Martínez Poyatos, D., Martín Parra, L.M., Mata, J., 2008. Rheic Ocean ophiolitic remnants in southern Iberia questioned by SHRIMP U-Pb zircon ages on the Beja-Acebuches amphibolites. Tectonics, 27, TC5006. DOI: https://doi.org/10.1029/2008TC002306

Bachmann, F., Hielscher, R., Schaeben, H., 2010. Texture analysis with MTEX - Free and open source software toolbox. Solid State Phenom, 160, 63-68, DOI: https://doi.org/10.4028/www.scientific.net/ssp.160.63

Barber, D.J., Wenk, H.R., Gomez-Barreiro, J., Rybacki, E., Dresen, G., 2007. Basal slip and texture development in calcite: new results from torsion experiments. Physics and Chemistry of Minerals, 34, 73-84. DOI: https://doi.org/10.1007/s00269-006-0129-3

Barnhoorn, A., Bystricky, M., Burlini, L., Kunze, K., 2004. The role of recrystallization on the deformation behaviour of calcite rocks: large strain torsion experiments on Carrara marble. Journal of Structural Geology, 26, 885-903. DOI: https://doi.org/10.1016/j.jsg.2003.11.024

Barnhoorn, A., Bystricky, M., Burlini, L., Kunze, K., 2005. Post-deformational annealing of calcite rocks. Tectonophysics, 403(1-4), 167-191. DOI: https://doi.org/10.1016/j.tecto.2005.04.008

Bestmann, M., Prior, D.J., 2003. Intragranular dynamic recrystallization in naturally deformed calcite marble: diffusion accommodated grain boundary sliding as a result of subgrain rotation recrystallization. Journal of Structural Geology, 25, 1597-1613. DOI: https://doi. org/10.1016/S0191-8141(03)00006-3

Bestmann, M., Kunze, K., Matthews, A., 2000. Evolution of a calcite marble shear zone complex on Thassos Island, Greece: microstructural and textural fabrics and their kinematic significance. Journal of Structural Geology, 22, 1789-1807. DOI: https://doi.org/10.1016/S0191-8141(00)00112-7

Bestmann, M., Prior, D.J., Grasemann, B., 2006. Characterization of deformation and flow mechanics around porphyroclasts in a calcite marble ultramylonite by means of EBSD analysis. Tectonophysics, 413, 185-200. DOI: https://doi.org/10.1016/j.tecto.2005.10.044

Boullier, A.M., Gueguen, Y., 1975. SP-Mylonites: Origin of some mylonites by superplastic flow. Contributions to Mineralogy and Petrology, 50, 93-104. DOI: https://doi.org/10.1007/BF00373329

Burkhard, M., 1993. Calcite twins, their geometry, appearance and significance as stress-strain markers and indicators of tectonic regime: a review. Journal of Structural Geology, 15(3-5), 351-368. DOI: https://doi.org/10.1016/0191-8141(93)90132-T

Burlini, L., Marquer, D., Challandes, N., Mazzola, S., Zangarini, N., 1998. Seismic properties of highly strained marbles from the Splügenpass, central Alps. Journal of Structural Geology, 20, 277-292. DOI: https://doi.org/10.1016/S0191-8141(97)00084-9

Busch, J.P., van der Pluijm, B.A., 1995. Calcite textures, microstructures and rheological properties of marbles in the Bancroft shear zone, Ontario, Canada. Journal of Structural Geology, 17, 677-688. DOI: https://doi.org/10.1016/0191-8141(94)00092-E

Carreras, J., Czeck, D.M., Druguet, E., Hudleston, P.J., 2010. Structure and development of an anastomosing network of ductile shear zones. Journal of Structural Geology, 32(5), 656-666. DOI: https://doi.org/10.1016/j.jsg.2010.03.013

Chichorro, M., Pereira, M.F., Díaz-Azpiroz, M., Williams, I.S., Fernández, C., Pin, C., Silva, J.B., 2008. Cambrian ensialic rift-related magmatism in the Ossa-Morena Zone (Évora-Aracena metamorphic belt, SW Iberian Massif): Sm-Nd isotopes and SHRIMP zircon U-Th-Pb geochronology. Tectonophysics, 461, 91-113. DOI: https://doi.org/10.1016/j.tecto.2008.01.008

De Bresser, H.J.P., 1989. Calcite c-axis textures along the Gavarnnie thrust zone, Central Pyrenees. Geologie en Mijnbouw, 68, 367-375.

De Bresser, J.H.P., Spiers, C.J., 1997. Strength characteristics of the r, f, and c slip systems in calcite. Tectonophysics, 272(1), 1-23. DOI: https://doi.org/10.1016/S0040-1951(96)00273-9

De Bresser, J., Urai, J., Olgaard, D., 2005. Effect of water on the strength and microstructure of Carrara marble axially compressed at high temperature. Journal of Structural Geology, 27, 265-281. DOI: https://doi.org/10.1016/j.jsg.2004.10.002

Dias da Silva, I., Pereira, M.F., Silva, J.B., Gama, C., 2018. Time-space distribution of silicic plutonism in a gneiss dome of the Iberian Variscan Belt: The Évora Massif (Ossa-Morena Zone, Portugal). Tectonophysics, 747, 298-317. DOI: https://doi.org/10.1016/j.tecto.2018.10.015

Dietrich, D., Song, H., 1984. Calcite fabrics in a natural shear environment, the Helvetic nappes of western Switzerland. Journal of Structural Geology, 6(1-2), 19-32. DOI: https://doi.org/10.1016/0191-8141(84)90080-4

Ebert, A., Herwegh, M., Berger, A., Pfifner, A., 2008. Grain coarsening maps for polymineralic carbonate mylonites: a calibration based on data from different Helvetic nappes (Switzerland). Tectonophysics, 457, 128-142. DOI: https://doi.org/10.1016/j.tecto.2008.05.007

Elyaszadeh, R., Sarkarinejad, K., Prior, D.J., 2017. Intracrystalline deformation of garnet, wollastonite and pectolite grains during development of a crenulation cleavage in the sheared skarn. Journal of Structural Geology, 101, 15-25. DOI: https://doi.org/10.1016/j.jsg.2017.06.010

Erskine, B.G., Heidelbach, F., Wenk, H.-R., 1993. Lattice preferred orientations and microstructures of deformed Cordilleran marbles: correlation of shear indicators and determination of strain path. Journal of Geology, 15(9-10), 1189-1205. DOI: https://doi.org/10.1016/0191-8141(93)90163-5

Felden, J., Möller, L., Schindler, U., Huber, R., Schumacher, S., Koppe, R., Diepenbroek, M., Glöckner, F.O., 2023. PANGAEA –Data Publisher for Earth & Environmental Science. Scientific Data, 10(1), 347. DOI: https://doi.org/10.1038/s41597-023-02269-x

Fossen, H., Cavalcante, G.C.G., 2017. Shear zones - A review. Earth Science Reviews, 171, 434-455. DOI: https://doi.org/10.1016/j.earscirev.2017.05.002

Ganino, C., Arndt, N.T., Chauvel, C., Tornos, F., 2014. Metamorphic degassing of carbonates in the contact aureole of the Aguablanca Cu–Ni–PGE deposit, Spain. Contributions to Mineralogy and Petrology, 168, 1053. DOI: https://doi.org/10.1007/s00410-014-1053-z

Gomes, M.C., 2000. Metamorfismo de Rochas Carbonatadas Siliciosas da Regiao de Alvito (Alentejo, Sul de Portugal). Ph.D. Thesis. Coimbra (Portugal), Universitat de Coimbra, 248pp.

Guillope, M., Poirier, J.P., 1979. Dynamic recrystallization during creep of single-crystalline halite: An experimental study. Journal of Geophysical Research, 84, 5557-5567. DOI: https://doi.org/10.1029/JB084iB10p05557

Hielscher, R., Schaeben, H., 2008. A novel pole figure inversion method: Specification of the MTEX algorithm. Journal of Applied Crystallography, 41(6), 1024-1037. DOI: https://doi.org/10.1107/s0021889808030112

Kurz, W., Neubauer, F., Unzog, W., Genser, J., Wang, X., 2000. Microstructural and textural development of calcite marbles during polyphase deformation of Penninic units within the Tauern Window (Eastern Alps). Tectonophysics, 316, 327-342. DOI: https://doi.org/10.1016/S0040-1951(99)00257-7

Kusbach, V.K., Machek, M., Roxerová, Z., Racek, M., Silva, P.F., 2019. Localization effect on AMS fabric revealed by microstructural evidence across small-scale shear zone in marble. Scientific Reports, 9, 17483. DOI: https://doi.org/10.1038/s41598-019-53794-y

Kusbach, V.K., Roxerová, Z., Machek, M., Kučeráková, M., Vratislav, S., Vávrová, A., Chadima, M. 2025a. AMS data of small scale marble shear zone, Viana do Alentejo, Ossa-Morena Zone, Portugal, complemented with microstructural and chemical data [dataset bundled publication]. PANGAEA, published: March 20th- DOI: https://doi.org/10.1594/PANGAEA.979680

Kusbach, V.K., Roxerová, Z., Machek, M., Kučeráková, M., Vratislav, S., Vávrová, A., Chadima, M., Silva, P.F., Racek, M., 2025b. The magnetic, microstructural and textural signature of shear zones in marbles and experimental simulations. ESS Open Archive, published: May 8th. DOI: https://doi.org/10.22541/essoar.174671883.37028240/v1

Leiss, B., Molli, G., 2003. 'High-temperature' texture in naturally deformed Carrara marble from the Alpi Apuane, Italy. Journal of Structural Geology, 25, 649-658. DOI: https://doi.org/10.1016/S0191-8141(02)00148-7

Lexa, O., Landa, D., 2024. ondrolexa/polylx: polylx 0.5.4 release (v0.5.4). Zenodo. Version: March 2024. DOI: https://doi.org/10.5281/zenodo.10781268

Mainprice, D., Bachmann, F., Hielscher, R., Schaeben, H., 2014. Descriptive tools for the analysis of texture projects with large datasets using MTEX: strength, symmetry and components. In: Faulkner, D.R., Mariani, E., Mecklenburgh, J. (eds.). Rock Deformation from Field, Experiments and Theory: A Volume in Honour of Ernie Rutter. London, The Geological Society, 409 (Special Publications), 251-271. DOI: http://dx.doi.org/10.1144/SP409.8

Marques, F., Machek, M., Roxerová, Z., Burg, J.-P., Almqvist, B., 2015. Mechanics, microstructure and AMS evolution of a synthetic porphyritic calcite aggregate deformed in torsion. Tectonophysics, 655, 41-57. DOI: https://doi.org/10.1016/j.tecto.2015.05.010

Means, W.D., 1995. Shear zones and rock history. Tectonophysics, 247, 157-160. DOI: https://doi.org/10.1016/0040-1951(95)98214-H

Molli, G., Conti, P., Giorgettil, G., Meccheri, M., Oesterling, N., 2000. Microfabric study on the deformational and thermal history of the Alpi Apuane marbles (Carrara marbles), Italy. Journal of Structural Geology, 22, 1809-1825. DOI: https://doi.org/10.1016/S0191-8141(00)00086-9

Moreira, N., Pedro, J., Santos, J.F., Araújo, A., Dias, R., Ribeiro, S., Romão, J., Mirão, J., 2019. 87Sr/86Sr applied to age discrimination of the Palaeozoic carbonates of the Ossa-Morena zone (SW Iberia Variscides). International Journal of Earth Sciences, 108, 963-987. DOI: https://doi.org/10.1007/s00531-019-01688-9

Oesterling, N., Heilbronner, R., Stünitz, H., Barnhoorn, A., Molli, G., 2007. Strain dependent variation of microstructure and texture in natu-rally deformed Carrara marble. Journal of Structural Geology, 29, 681-696. DOI: https://doi.org/10.1016/j.jsg.2006.10.007

Ohl, M., Nzogang, B., Mussi, A., Wallis, D., Drury, M., Plümper, O., 2021. Crystal-plastic deformation in seismically active carbonate faultrocks. Journal of Geophysical Research: Solid Earth, 126(4), e2020JB020626. DOI: https://doi.org/10.1029/2020JB020626

Panozzo, R., 1983. Two-dimensional analysis of shape-fabric using projections of digitized lines in a plane. Tectonophysics, 95, 279-294. DOI: https://doi.org/10.1016/0040-1951(83)90073-2

Panozzo, R., 1984. Two-dimensional strain from the orientation of lines in a plane. Journal of Structural Geology, 6(1-2), 215-221. DOI: https://doi.org/10.1016/0191-8141(84)90098-1

Panozzo, R., Hürlimann, H., 1983. A simple method for the quantitative discrimination of convex and convex-concave lines. Microscopica Acta, 87(2), 169-176.

Pereira, M.F., Silva, J.B., Chichorro, M., Moita, P., Santos, J.F., Apraiz, A., Ribeiro, C., 2007. Crustal growth and deformational processes in the Northern Gondwana margin: Constraints from the Évora Massif (Ossa-Morena Zone, SW

Iberia, Portugal). In The Evolution of the Rheic Ocean: From Avalonian–Cadomian Active Margin to Alleghenian-Variscan Collision. In: Linnemann, U., Nance, R.D., Kraft, P., Zulauf, G. (eds.). Boulder (Colorado, USA), Geological Society of America, 423, 333-358.

Pereira, M.F., Chichorro, M., Williams, I.S., Silva, J.B., Fernandez, C., Diaz-Azpiroz, M., Apraiz, A., Castro, A., 2009. Variscan intra-orogenic extensional tectonics in the Ossa-Morena Zone (Évora-Aracena-Lora del Rio metamorphic belt, SW Iberian Massif): SHRIMP zircon U-Th-Pb geochronology. In Ancient Orogens and Modern Analogues. In: Murphy, J.B., Keppie, J.D., Hynes, A.J. (eds.). Boulder (Colorado, USA), Geological Society of America, 327, 215-237.

Pereira, M.F., Chichorro, M., Silva, J., Ordóñez-Casado, B., Lee, J., Williams, I., 2012. Early Carboniferous wrenching, exhumation of high-grade metamorphic rocks and basin instability in SW Iberia; constraints derived from structural geology and U–Pb and 40Ar-39Ar geochronology. Tectonophysics, 558, 28-44. DOI: https://doi.org/10.1016/j.tecto.2012.06.020

Pereira, M.F., Chichorro, M., Moita, P., Santos, J.F., Solá, A.M.R., Williams, I.S., Silva, J.B., Armstrong, R.A., 2015. The multistage crystallization of zircon in calc-alkaline granitoids: U-Pb age constraints on the timing of Variscan tectonic activity in SW Iberia. International Journal of Earth Sciences, 104, 1167-1183. DOI: https://doi.org/10.1007/s00531-015-1149-3

Pereira, M.F., Fuenlabrada, J.M., Rodríguez, C., Castro, A., 2022. Changing Carboniferous Arc Magmatism in the Ossa-Morena Zone (Southwest Iberia): Implications for the Variscan Belt. Minerals, 12, 597. DOI: https://doi.org/10.3390/min12050597

Piazolo, S., Prior, D.J., Holness, M.D., Harstad, A.O., 2007. Annealing in a natural laboratory: an EBSD and Cl study of calcite and quartz growth from volumes of rock heated by a nearby melt intrusion. Material Science Forum, 550, 333-338. DOI: https://doi.org/10.4028/www.scientific.net/MSF.550.333

Pieri, M., Burlini, L., Kunze, K., Stretton, I., Olgaard, D.L., 2001a. Rheological and microstructural evolution of Carrara marble with high shear strain: results from high temperature torsion experiments. Journal of Structural Geology, 23, 1393-1413. DOI: https://doi.org/10.1016/s0191-8141(01)00006-2

Pieri, M., Kunze, K., Burlini, L., Stretton, I., Olgaard, D.L., Burg, J.-P., Wenk, H.-R., 2001b. Texture development of calcite by deformation and dynamic recrystallization at 1000 K during torsion experiments of marble to large strains. Tectonophysics, 330, 119-140. DOI: https://doi.org/10.1016/S0040-1951(00)00225-0

Pin, C., Fonseca, P.E., Paquette, J.-L., Castro, P., Matte, P., 2008. The ca. 350 Ma Beja Igneous Complex: a record of transcurrent slab break-off in the Southern Iberia Variscan Belt? Tectonophysics, 461, 356-377. DOI: https://doi.org/10.1016/j.tecto.2008.06.001

Poirier, J.P., 1985. Creep of crystals. High temperature deformation processes in metals, ceramics and minerals. Cambridge, Cambridge University Press, 260pp.

Quesada, C., 1992. Evolución tectónica del Macizo Ibérico (Una historia de crecimiento por acrecencia sucesiva de terrenos durante el Proterozoico superior y el Paleozoico). In: Gutiérrez-Marco, J.C., Saavedra, J., Rábano, I. (eds.). Palaeozoico inferior de Ibero-América. University of Extremadura, 173-190.

Quesada, C., 2006. The Ossa-Morena Zone of the Iberian Massif: a tectonostratigraphic approach to its evolution. Zeitschrift der Deutschen Gesellschaft für Geowissenschaften, 157, 585-595.

Quesada, C., Oliveira, J.T., 2019. The geology of Iberia: A geodynamic approach, Volume 2: The Variscan Cycle. Springer International Publishing, 544pp.

Ramsay, J.G., 1980. Shear zone geometry: a review. Journal of Structural Geology, 1-2, 83-99. DOI: https://doi.org/10.1016/0191-8141(80)90038-3

Ramsay, J.G., Graham, R.H., 1970. Strain variation in shear belts. Canadian Journal of Earth Sciences, 7, 786-813. DOI: https://doi.org/10.1139/e70-078

Ramsay, J.G., Huber, M.I., 1983. The techniques of modern structural geology: strain analysis. Academic press, volume 1, 307pp.

Ribeiro, A., Quesada, C., Dallmeyer, R., 1990. Geodynamic evolution of the Iberian Massif. Pre-Mesozoic geology of Iberia. Berlin, Springer, 399-409.

Rosas, F., Marques, F., Ballevre, M., Tassinari, C., 2008. Geodynamic evolution of the SW Variscides: Orogenic collapse shown by new tectonometamorphic and isotopic data from western Ossa-Morena Zone, SW Iberia. Tectonics, 27, TC6008. DOI: https://doi.org/10.1029/2008TC002333

Roxerová, Z., Kusbach, V., Machek, M., Kučeráková, M., Vratislav, S., Vávrová, A., Chadima, M., 2025. Effect of deformation mechanisms on magnetic record in marble shear zones. Geochemistry, Geophysics, Geosystems, 26, e2025GC012456. DOI: https://doi.org/10.1029/2025GC012456

Rutter, E.H., Casey, M., Burlini, L., 1994. Preferred crystallographic orientation development during the plastic and superplastic flow of calcite rocks. Journal of Structural Geology, 16(10), 1431-1446. DOI: https://doi.org/10.1016/0191-8141(94)90007-8

Rybacki, E., Morales, L.F.G., Naumann, M., Dresen, G., 2014. Strain localization during high temperature creep of marble: the effect of inclusions. Tectonophysics, 634, 182-197. DOI: https://doi.org/10.1016/j.tecto.2014.07.032

Schenk, O., Urai, J.L., Evans, B., 2005. The effect of water on recrystallization behavior and grain boundary morphology in calcite-observations of natural marble mylonites. Journal of Structural Geology, 27(10), 1856-1872. DOI: https://doi.org/10.1016/j.jsg.2005.05.015

Schmid, S.M., Panozzo, R., Bauer, S., 1987. Simple shear experiments on calcite rocks: rheology and microstructure. Journal of Structural Geology, 9(5-6), 747-778. DOI: https://doi.org/10.1016/0191-8141(87)90157-X

Schmid, S.M., Paterson, M.S., Boland, J.N., 1980. High temperature flow and dynamic recrystallization in carrara marble. Tectonophysics, 65(3-4), 245-280. DOI: https://doi.org/10.1016/0040-1951(80)90077-3

Schulmann, K., Maierová, P., Jeřábek, P., Lexa, O., Ulrich, S., Hobbs, B., Ord, A., 2023. Deformation mechanisms and rheology inversion of jointly deformed marble and quartzite in natural thermal gradient. Journal of Structural Geology, 173, 104892. DOI: https://doi.org/10.1016/j.jsg.2023.104892

Sibson, R.H., 1977. Fault rocks and fault mechanisms. Journal of The Geological Society, 133, 191-213. DOI: https://doi.org/10.1144/gsjgs.133.3.0191

Skemer, P., Katayama, I., Jiang, Z., Karato, S.I., 2005. The misorientation index: development of a new method for calculating the strength of lattice-preferred orientation. Tectonophysics, 411, 157-167. DOI: 10.1016/j.tecto.2005.08.023

Stipp, M., Stünitz, H., Heilbronner, R., Schmid, S.M., 2002. The eastern Tonale fault zone: A "natural laboratory" for crystal-plastic deformation of quartz over a temperature range from 250 to 700°C. Journal of Structural Geology, 24(12), 1861-1884. DOI: https://doi.org/10.1016/S0191-8141(02)00035-4

Stünitz, H., Fitz Gerald, J.D., 1993. Deformation of granitoids at low metamorphic grades. II. Granular flow in albite-rich mylonites. Tectonophysics, 221, 299-324. DOI: https://doi.org/10.1016/0040-1951(93)90164-F

Sánchez-García, T., Quesada, C., Bellido, F., Dunning, G., Pin, C., Moreno-Eiris, E., Perejón, A., 2016. Age and characteristics of the Loma del Aire unit (SW Iberia): implications for the regional correlation of the Ossa-Morena Zone. Tectonophysics, 681, 58-72.

Urai, J.L., Means, W.D., Lister, G.S., 1986. Dynamic recrystallization of minerals. In: Hobbs, B.E., Heard, H.C. (eds.). Mineral and Rock Deformation: Laboratory Studies (The Paterson Volume). Geophysical Monograph of American Geophysical Union, 36, 161-200.

Van der Pluijm, B.A., 1991. Marble mylonites in the Bancroft shear zone, Ontario, Canada: microstructures and deformation mechanisms. Journal of Structural Geology, 13(10), 1125-1135. DOI: https://doi.org/10.1016/0191-8141(91)90073-R

Wenk, H.-R., 2002. Texture and anisotropy. In: Karato, S., Wenk, H.-R. (eds.). Plastic Deformation of Minerals and Rocks. Reviews in Mineralogy and Geochemistry, 51, 291-352. DOI: https://doi.org/10.2138/gsrmg.51.1.291

Wenk, H.-R., Takeshita, T., Bechler, E., Erskine, B.G., Matthies, S., 1987. Pure shear and simple shear calcite textures. Comparison of experimental, theoretical and natural data. Journal of Structural Geology, 9(5-6), 731-745. DOI: https://doi.org/10.1016/0191-8141(87)90156-8

Manuscript received May 2025;
revision accepted September 2025;
published Online October 2025.

ARTICLE IN PRESS

APPENDIX

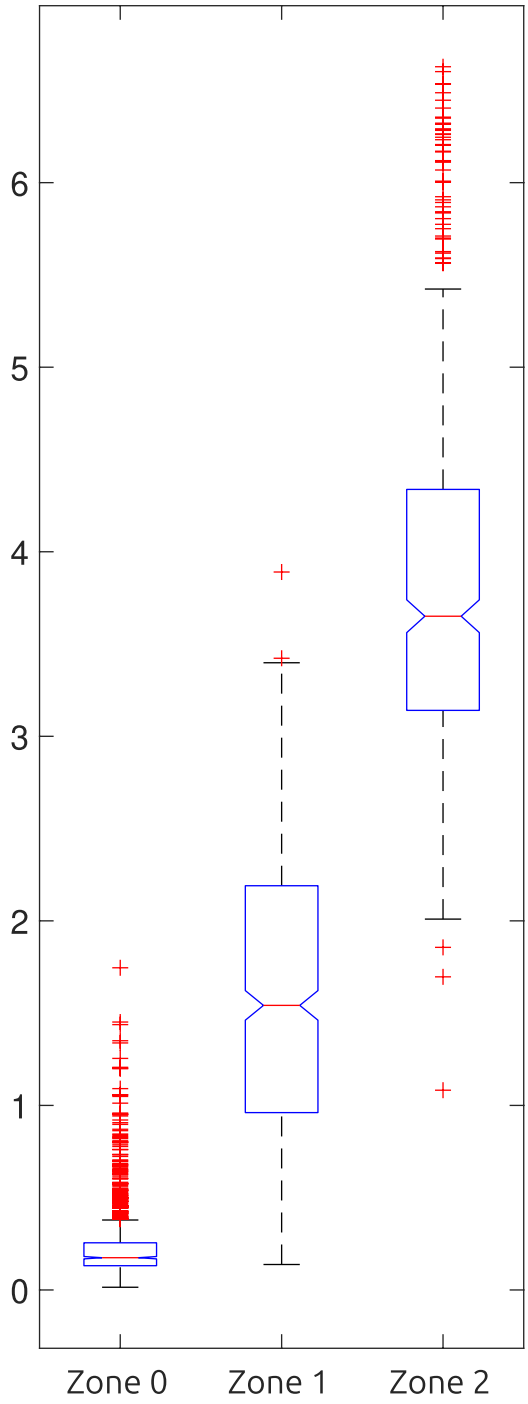

Statistical description

Zone 2	
Mean	3.869
Median	3.6507
St. Dev.	1.0628
Variance	1.1295
Minimum	1.0823
Maximum	6.6281

Zone 1	
Mean	1.6008
Median	1.542
St. Dev.	0.77677
Variance	0.60337
Minimum	0.13795
Maximum	3.8903

Zone 0	
Mean	0.23869
Median	0.17478
St. Dev.	0.21142
Variance	0.044697
Minimum	0.014641
Maximum	1.7458

FIGURE I. Box and whisker plots showing statistical strain analysis across three defined zones: Zone 0 (undeformed), Zone 1 (curved primary foliation) and Zone 2 (fabric reoriented parallel to the SZ).

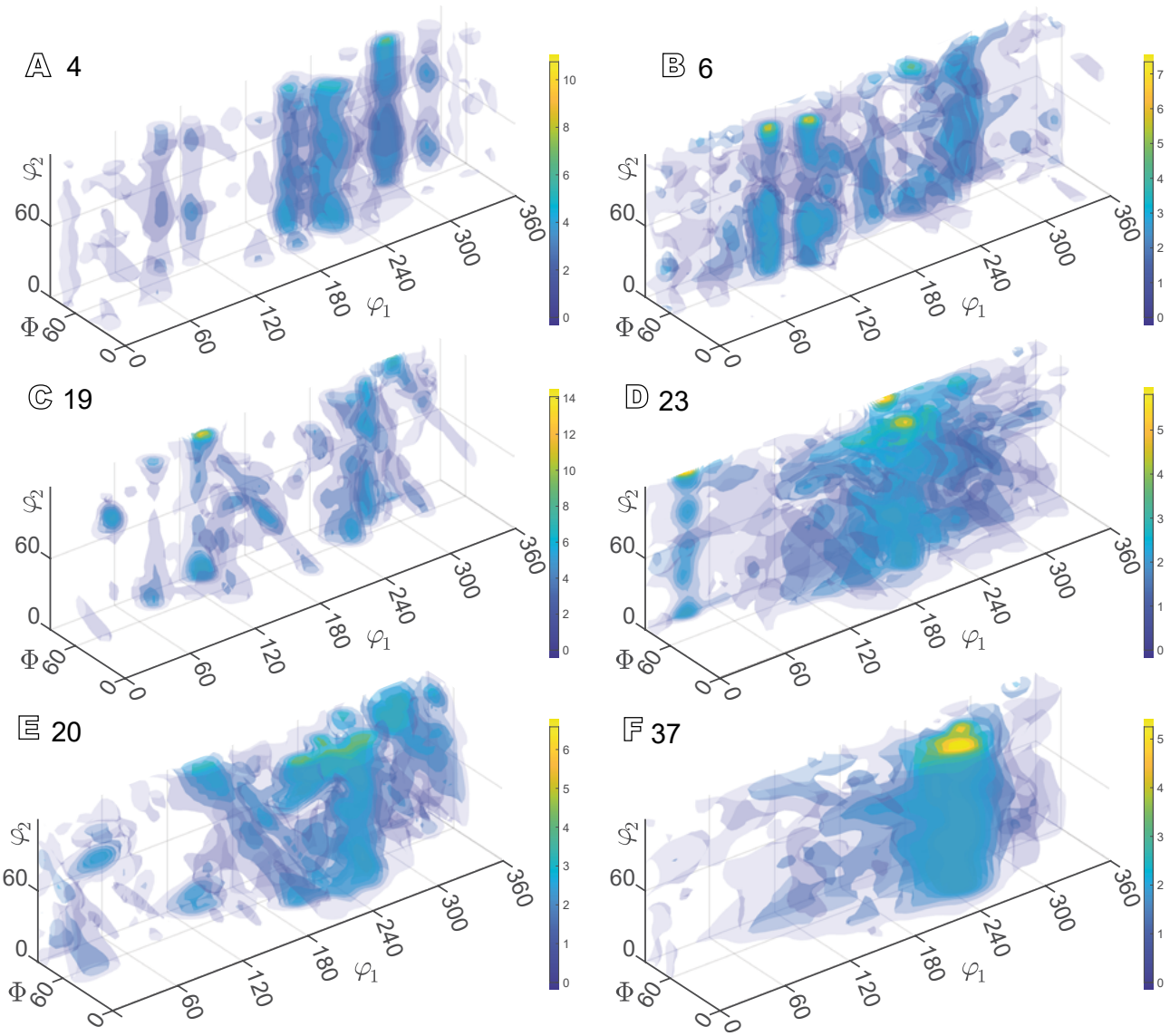

FIGURE II. Orientation Distribution Functions (ODFs) determined by ND in 3D Euler angle space representation.

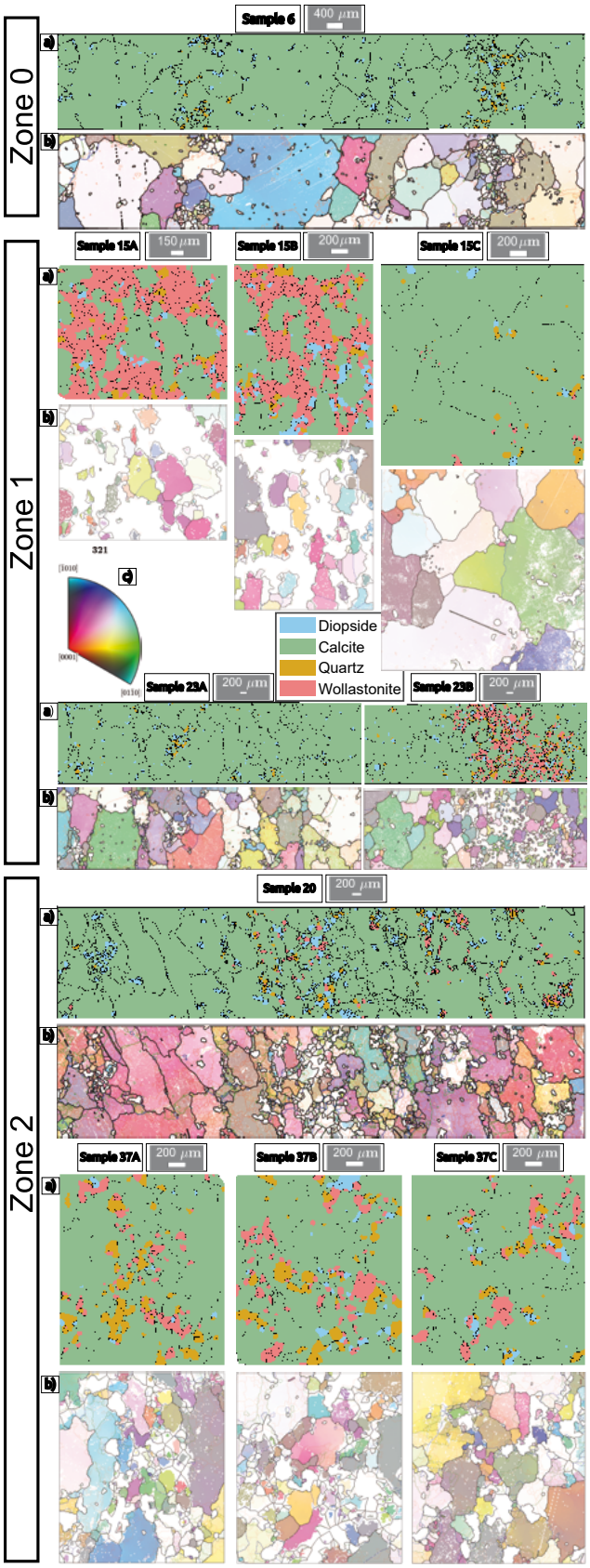

FIGURE III. EBSD phase maps and maps of calcite grain and subgrain boundaries. Grain boundary (black) defined by misorientation greater than 10°. Subgrain boundaries defined at three levels of misorientation 0.5° in red, 1° in blue and 2° in green.

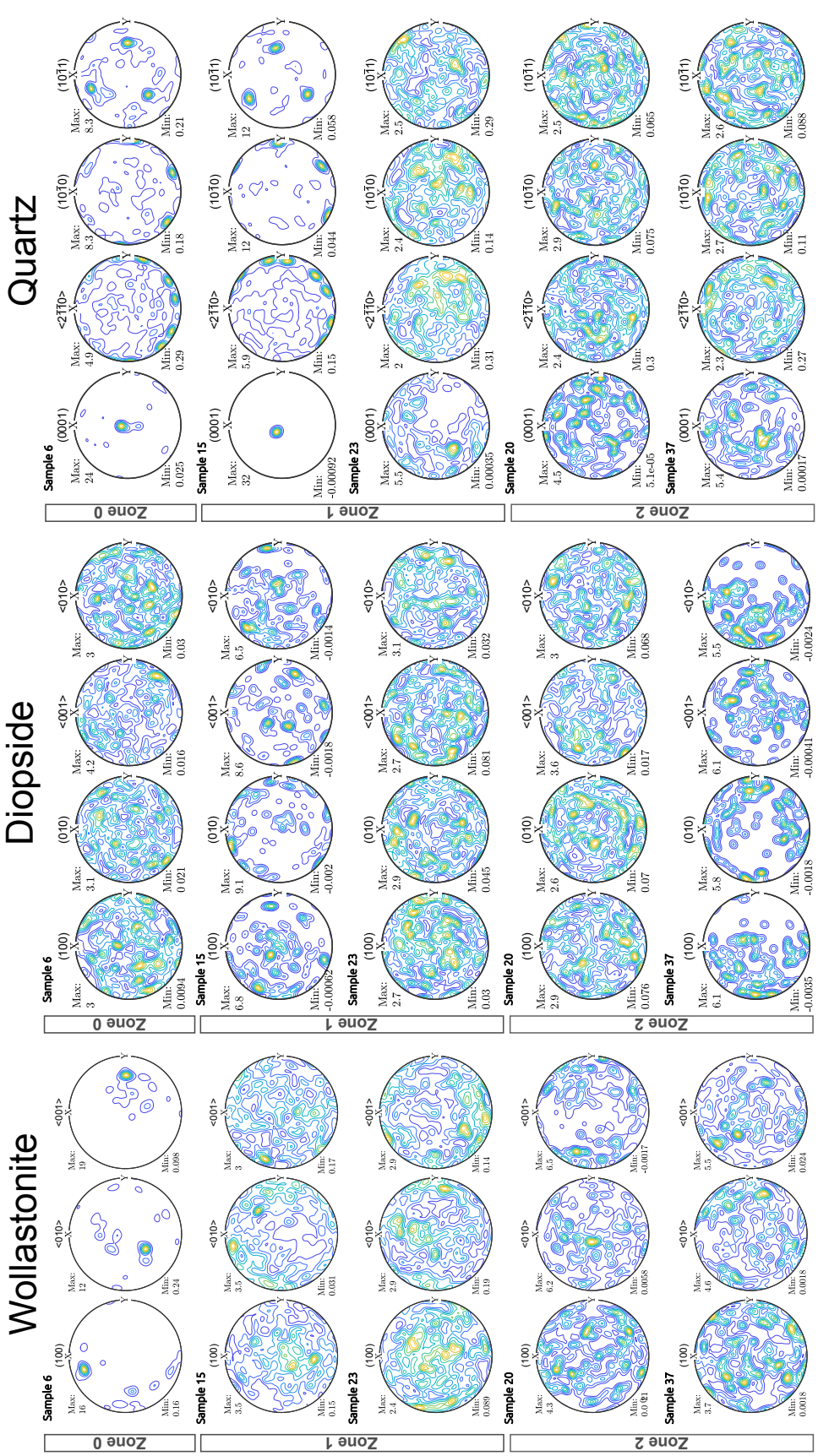

FIGURE IV. CPO pole figures for main crystallographic directions of secondary phases wollastonite, quartz and diopside from EBSD measurements.

ARTICLE IN PRESS

TABLE I. Quantitative microstructural parameters of calcite in different samples/zones. Measurements include modal composition (area %), Equivalent Area Diameter (EAD, in mm), Aspect Ratio (AR), Percentile Average Relative Indented Surface (PARIS) factor, Surface and Particle Orientation Ratios (SURFOR and PAROR) and fabric strength indices (M-index and J-index). Mean, median, and modal values are reported for grain size and shape parameters

Sample		**6** c1-6-2	**4** c1-4-2	**4+6** c1-6-2 and c1-4-2	**16** c1-16-4	**19** C1-19-3	**23** c1-23-3	**20** c1-20-1	**37** c1-37-1
Zone		**0**			**1**			**2**	
Modal Composition	*calcite*	97.93	96.19	97.12	89.76	99.91	95.15	97.33	95.16
	aggr	2.07	3.81	2.88	10.24	0.09	4.85	2.67	4.84
EAD *Calcite*	*mean*	1.019	0.889	0.955	0.613	0.860	0.730	0.716	0.422
	median	0.741	0.609	0.670	0.483	0.701	0.618	0.587	0.329
	mode	0.511	0.473	0.472	0.374	0.558	0.417	0.424	0.217
AR *Calcite*	*mean*	1.760	1.800	1.780	1.703	1.804	1.746	1.792	1.827
	median	1.623	1.696	1.662	1.586	1.658	1.628	1.674	1.670
	mode	1.459	1.476	1.452	1.395	1.489	1.407	1.532	1.454
PARIS *Calcite*	*mean*	15.050	15.884	15.464	10.231	9.370	12.151	11.647	10.436
	median	7.982	8.492	8.227	6.770	6.268	8.015	7.820	6.559
	mode	6.003	6.337	5.767	4.294	3.251	5.200	5.593	3.278
SURFOR *Calcite*	*max*	0.888	0.903		0.899	0.901	0.898	0.894	0.889
	min	0.752	0.725		0.750	0.730	0.750	0.740	0.751
PAROR *Calcite*	*max*	0.911	0.922		0.917	0.917	0.917	0.919	0.908
	min	0.782	0.747		0.766	0.746	0.769	0.761	0.767
M index *Calcite*		0.042	0.021			0.052	0.054	0.044	0.069
J index *Calcite*		1.341	1.458			1.542	1.322	1.361	1.334